Assessment of Human Dynamic Gait Stability with a Lower Extremity Assistive Device

Prudhvi Tej Chinimilli, Seyed Mostafa Rezayat Sorkhabadi, and Wenlong Zhang*, *Member, IEEE*

***Abstract*— This paper focuses on assessing gait stability by metrics derived from dynamical systems theory to understand the influence of unilateral robot assistance on the human walking pattern. A motorized assistive robot is applied to the right knee joint to provide stance support. The metrics related to global stability (the maximum Floquet multiplier, max FM), local stability (short-term and long-term divergence exponents, λ_s and λ_l), and variability (median absolute deviation, MAD) are considered. These metrics are derived for bilateral hip, knee, and ankle joint angles. Additionally, a biomechanical metric, the minimum margin of stability is assessed. Experiments are conducted on 11 healthy participants with different robot controllers. The max FM and λ_s yield statistically significant results, showing that the unassisted (left) leg is more stable in right knee assistance conditions when compared to the normal walking condition due to inter-limb coordination. Moreover, MAD and λ_l show that the variability and chaotic order of walking pattern during assistance are lower than those of normal walking. The proposed control strategy (automatic impedance tuning, AIT) improves local and orbital gait stability compared to existing controllers such as finite-state machine (FSM). The assessment of dynamic gait stability presented in this paper provides insights for further improving control strategies of assistive robots to help a user reach improved gait stability while maintaining appropriate variability.**

***Index Terms*— Dynamic stability, Nonlinear dynamics, Assistive devices, Rehabilitation, Biomechanics**

I. Introduction

A survey from the United Nations shows that people older than 60 are 11.5% of the global population in 2012, and this number will be nearly doubled by 2050 [1]. Aging is reflected by reduced physical capabilities due to physiological changes. The reduced physical performance due to muscle deterioration, loss of motor units, and reduced neuromuscular activation may lead to gait disorders in senior adults [2]. Similar problems are prevalent in patients with neurological diseases such as stroke and spinal cord injury. Current research mainly focuses on developing wearable lower-extremity assistive devices (LEADs) that help the users improve their walking performance and restore impaired motor control [3]–[5].

One major concern for senior citizens is falling during walking [6]. In the aforementioned examples for LEADs, the main focus is put on providing assistance to improve walking performance. Muscle activity and metabolic cost are measured to evaluate the level of assistance provided by LEAD to the human [4]. However, there has not been enough assessment of dynamic gait stability for the combined human-LEAD system [4], [5], [7]. The LEAD as an external device may induce perturbations to the human body and may influence the inherent stability of the human. Therefore, it is important to introduce stability metrics and assess the overall dynamic gait stability of the human-LEAD system.

A. Chaos and Optimal Variability

Human gait is not strictly periodic. Any variations from the periodic pattern were traditionally considered as noise in the neuromuscular system [8]. However, later investigations showed that these variations follow a chaotic structure [9]. To understand gait variability, a theoretical model (predictability versus complexity) was proposed to explain movement variability as it was related to motor learning and health [10]. The model is based on the idea that mature motor skills are associated with optimal movement variability that reflects the adaptability of the underlying control system. Practically at the optimal state of movement variability (chaotic block shown in Fig. 1), the biological system is in a healthy state and is characterized by exhibiting chaotic temporal variations. This state lies in the intermediate region between excessive order (i.e., maximum predictability) and excessive disorder (i.e., no predictability). Thus this variability has a deterministic structure and reflects the adaptability of the system. This model provides an explanation for the neuromuscular control of the human gait, which implies that the stride to stride variability follows the chaotic structure, i.e., optimal variability. This system has an ergodic property, meaning that the trajectories come close to a fixed point's neighborhood but never converge to the specific point. Therefore, the stability metrics related to chaos and nonlinear dynamics will be useful for assessing the human gait stability.

B. Related Work on Stability Metrics

Although many gait stability criteria have been proposed, there is still no commonly accepted method to assess locomotion stability. Most of these metrics reflect the ability of the system to respond to large perturbations (such that the system states stay in a safe range), and how quickly the system can respond to perturbations [11]. Nevertheless, these measures

*Address all correspondence to this author.
The authors are with the The Polytechnic School, Ira A. Fulton Schools of Engineering, Arizona State University, Mesa, AZ, 85212, USA. E-mail: {Prudhvi.Chinimilli, srezayat, Wenlong.Zhang}@asu.edu.
The first two authors contributed equally to this work.
This work was supported in part by the National Science Foundation under Grant IIS-1756031.

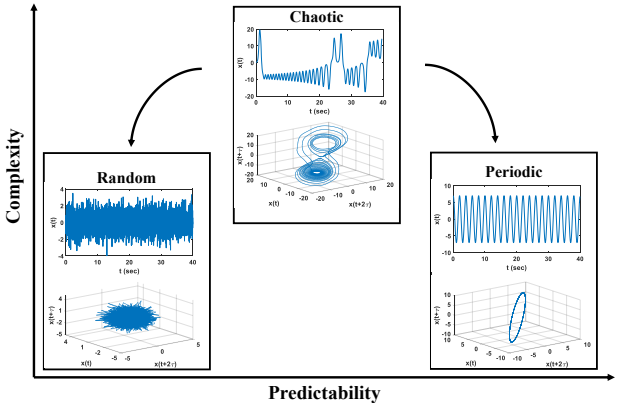

Fig. 1. Theoretical model for optimal variability illustrated using random, chaotic, and periodic signals. Behavior in terms of variability should be viewed in a continuum as being more or less predictable (on the x-axis) and as being more or less complex (on the y-axis).

can still correlate to the likelihood of falls as they quantify how a system responds to perturbations [11].

There are metrics derived from dynamical systems theory for gait stability assessment. The computation of these metrics is based on the time series data of kinematics and/or gait parameters. Dingwell et al. used the maximum Lyapunov exponent (max LE, λ) to quantify gait stability [12], by calculating the average logarithmic rate of divergence of the system after a small perturbation. For chaotic systems, λ is always positive, with less indicating less instability. In many gait studies, the max LE is defined over two regions, 0 to 1 stride (labeled as λ_s) and 4 to 10 strides (labeled as λ_l). Lockhart and Liu reported a larger λ_s in fall-prone elderly subjects than healthy elderly subjects [13]. McAndrew et al. reported that gait destabilization, by means of support surface perturbations or visual scene perturbations, was reflected in λ_s but probably not in λ_l [14]. In summary, these findings obtained in previous experimental studies suggest λ_s as a valid indicator to estimate the probability of falling.

Another measure derived from the dynamic systems theory is orbital stability [15], which is defined by computing the maximum Floquet multiplier (max FM) to quantify the rate of convergence or divergence of continuous gait variables (e.g., segmental motions and joint angles) towards a limit cycle (e.g., the nominal gait cycle). The system with a max FM value less than 1 is considered stable. Granata and Lockhart reported that the max FM was larger in a group of four fall-prone elderly subjects who had a self-reported history of falling than four healthy elderly subjects [16]. In [14], the max FM showed higher values (less orbital stability) in visual perturbation experiments which were designed for gait destabilization. However, in [17], the max FM did not correspond to the probability of falling. The concept of orbital stability showed mixed results in concerning the probability of falling. Some used the variability of certain parameters over strides as a measure to assess stability during walking. The median absolute deviation (MAD) was proposed as a measure for gait variability [18].

In addition to the measures from the dynamical systems theory, biomechanical measures were commonly used to assess stability during gait. The extrapolated center of mass (margin of stability) was derived for subjects walking on destabilized environments using platform oscillations and visual perturbations [19]. Others used the concept of stabilizing and destabilizing forces to assess gait stability [20].

C. Motivation and Contribution

There is limited literature that focuses on assessing the impact of exoskeleton design and control on gait variability and gait stability. In [21], FM and λ_l metrics were used to evaluate the influence of an ankle exoskeleton on gait variability. In another study, an increased max FM of ankle joint kinematics with exoskeleton assistance was reported, compared to walking without exoskeleton [22]. In this paper, the focus is put on the influence of a knee assistive device (KAD) on the inherent dynamic gait stability of the user, with different stability metrics (including biomechanical measures) and control approaches for the KAD.

The goal of this study is to bring insights by using stability metrics for further improving the dynamic stability of walking with LEADs. Five walking conditions are considered to demonstrate the impacts of design and different control strategies of KAD. The walking conditions include three that are non-assistive (normal, passive, and zero impedance, ZI) and two that are assistive (finite state machine, FSM, and automatic impedance tuning, AIT). The passive and ZI modes reveal the impacts of friction and inertia of KAD. FSM is a widely adopted strategy to modulate the impedance parameters in the robot controller based on gait phases [23], [24]. The AIT approach was developed in our previous work [25]. It adopts the same virtual impedance for each gait phase as the FSM, but the impedance values are smoothed during the transition between two gait phases. In this study, 11 participants (8 male, 3 female) are recruited and their walking stability is analyzed under the five conditions. The contributions of the paper are as follows:

1) Different stability metrics are assessed to describe the influence of robot assistance on the dynamic gait stability of the user. Local and orbital stability, kinematic variability, and margin of stability are used as the metrics.
2) The effects of unilateral assistance (applied to the right knee) on intra, and inter lower-limb joints are demonstrated using max FM and λ_s. We observe that the unassisted (left) leg is more stable when the right knee is assisted, compared to the normal walking condition due to inter-limb coordination.
3) Performance of our proposed control strategy (AIT) is compared with FSM using stability metrics. AIT results in improved orbital and local stability than FSM, which can be attributed to the smooth transition of robot assistance between gait phases.

The aforementioned contributions will shed light on how wearable robots alter the gait stability of the user. Firstly, this study compares different stability metrics and provides quantitative tools to evaluate the influence of wearable robots on the gait stability and variability of the users. This will help physical therapists design personalized training strategies for a

given patient and reduce falls during robot-aided gait training. Secondly, this study shows that it is possible to assess the control strategies of wearable robots using gait stability metrics. Thus, gait stability assessment will lead to improved control strategies of the wearable robot and more stable human-robot systems. Finally, the inter-limb coordination demonstrated in this paper will encourage more studies to understand the mechanism and design more effective training protocols with assistive robots.

The rest of the paper is organized as follows: Section II gives details about the hardware and protocol used in the experiments. Section III introduces the stability metrics derived from dynamical systems theory and biomechanics. Section IV discusses the results of stability metrics for all the experimental conditions. Section V discusses the results and the effects of unilateral assistance on both legs, as well as some limitations of the study. Section VI concludes this paper and presents some future work.

II. Methods

A. Hardware Design

The KAD design targets users with a unilateral impairment which affects their knee functions. The KAD is an exoskeleton with a compact rotary series elastic actuator (cRSEA) which weights around 1.57 is designed to assist the right knee. Maxon RE40, a 150W DC Motor is used to power the KAD. With a combined gear set reduction ratio of 63.6:1, the end effector can reach a maximum angular velocity of 120 rpm and the KAD can provide a maximum continuous assistive torque of 11.26 N·m. More details on the hardware and control structure of the KAD are given in [25].

The smart shoes are developed to measure ground contact forces (GCFs) at four points: heel, first metatarsal joint (Meta 1), fourth metatarsal joint (Meta 4) and toe. Silicone tubes are wound into air bladders and connected to barometric pressure sensors. The sampling rate of the smart shoes is set to 100 Hz and a model-based filter is implemented to compensate for hysteresis and estimate GCFs from pressure sensor readings in real time [26]. Gait phases are detected using a fuzzy logic based algorithm developed in [27].

B. Control Strategies

As mentioned in Section I-C, the experiments consist of five sessions with different control strategies: normal walking, passive, ZI, FSM, and AIT. In the passive case, the KAD is not powered and was driven by the user. In the ZI case, the KAD is powered but the virtual impedance parameters are set to zero, meaning that the motor just compensates for its own inertia by actively tracking the knee angle of the user without providing assistance. In FSM and AIT conditions, the KAD provides assistive torque to the right knee. The virtual impedance parameters for FSM and AIT conditions are chosen according to the identified quasi-stiffness and damping for each participant. A spring-damper model is considered for modeling the human knee torque with respect to the knee angle and angular velocity [28]:

TABLE I
THE DETAILS OF HEALTHY PARTICIPANTS VOLUNTEERED FOR THE EXPERIMENTS. R - RIGHT AND L - LEFT.

ID	Gender	Age	Height (cm)	Weight (kg)	Dominant Leg (R/L)
1	Male	23	180	60	R
2	Male	20	175	94	R
3	Male	25	178	69	R
4	Male	22	182	62	R
5	Male	24	173	62	R
6	Male	26	172	67	R
7	Male	29	165	70	R
8	Male	20	175	79	R
9	Female	27	154	54	R
10	Female	23	152	62	R
11	Female	28	160	65	R

$$T_h(t) = k \cdot (\theta_h(t) - \theta_0) + b \cdot \dot{\theta}_h(t), \tag{1}$$

where $T_h(t)$, $\theta_h(t)$, and $\dot{\theta}_h(t)$ are the human knee torque, angle, and angular velocity, respectively. k, b, and θ_0 represent the knee stiffness, damping, and setpoint, respectively. A gait cycle can be divided into two main phases: stance (ST) and swing (SW). The ST can be further divided into three subphases: stance flexion (SF), mid stance (MST) and terminal stance (TST). In this paper, k, b, and θ_0 are identified for three phases SF, MST, and TST using a least squares method with $T_h(t)$ as the output and $\theta_h(t)$, $\dot{\theta}_h(t)$ as the inputs. For the FSM case, the virtual impedance for each of the gait phases is predefined as 10% of the quasi-stiffness and damping calculated for each participant. The assistive torque is set based on an impedance control law with the same structure as (1), but the k and b are the virtual impedance of the robot in this case. In order to avoid sudden jumps in the robot impedance during transitions between two phases, an AIT controller was proposed [25]. In the AIT controller, the same robot impedance value for each gait phase is used as the FSM case, but the impedance is smoothed with a probabilistic inference of gait phases using a Gaussian mixture model (GMM).

C. Experimental Protocol

The experiments for this paper were set up in the motion capture laboratory equipped with 10 high-speed infrared cameras (Vicon Motion Systems Ltd., Oxford, England) and an instrumented treadmill (Bertec Corp., Ohio) at Arizona State University (ASU). The ASU Institutional Review Board (IRB) reviewed and approved this study (STUDY00007601). Details of the eleven healthy participants (8 male and 3 female) volunteered in this experiment are given in Table I. All the participants are right leg dominant because of our KAD design. The slope and speed of the treadmill for the walking experiments were set to 0 degrees and 0.8 m/s, respectively. Each session lasted for three minutes. The participants relaxed for 15 minutes before starting the next session. All the sessions for one participant were completed on a single day, and the order of these sessions was randomized. The experiment setup for the participant walking on the treadmill is shown in Fig. 2. Each participant wore 16 reflective markers, KAD, and smart shoes. The Vicon cameras captured marker positions at a frame

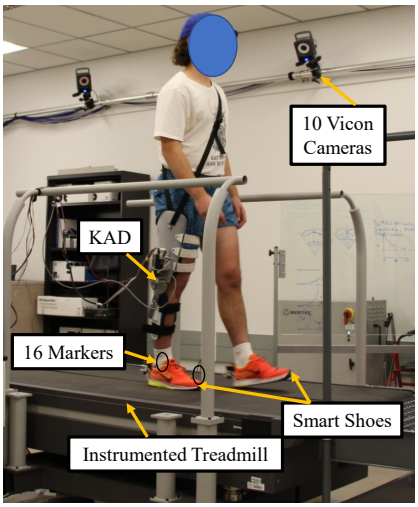

Fig. 2. Experiment setup: participant walking on the instrumented treadmill wearing reflective markers, smart shoes, and KAD.

rate of 100 Hz, while the instrumented treadmill captured 3D GCFs at 1,000 Hz.

III. Stability Metrics

A. Measures from Dynamical Systems Theory

There are two types of stability: global or orbital stability, and local stability. Global stability refers to the ability of a system to accommodate finite perturbations. Whereas, local stability refers to the sensitivity of the system to infinitesimally small perturbations. In this section, three measures derived from dynamical systems theory are described, namely the max LE, max FM, and MAD. These measures are generally computed from a steady-state walking pattern without external perturbations. These metrics can be used to assess gait stability when there are perturbations [14], [29].

1) State space reconstruction: To study the dynamics behind the gait kinematics, we need to construct a corresponding state space. For mechanical systems, the states are usually the positions and velocities of the system components. However, human gait is a complex dynamic system with strong nonlinearities and uncertainties. Therefore we need to reconstruct the state space for each time series from the original data and time-delayed copies using standard techniques given in [30]

$$s(t) = [x(t), x(t+\tau), x(t+2\tau), ..., x(t+(d_E-1)\tau)]^T, \quad (2)$$

where $s(t) \in \mathbb{R}^{d_E}$, and $x(t) \in \mathbb{R}$ is the original one-dimensional data. τ and d_E are the time delay and embedding dimension, respectively. The time delays are calculated from the first minimum of the average mutual information (AMI) function and the embedding dimensions are determined from global false nearest neighbors (GFNN) analysis [30]. An example for the computation of d_E and τ is shown in Figs. 3 (b) and (c). In Fig. 3(b), the FNN (%) does not change for $d_E > 5$. This implies the optimal d_E for time series signal $x(t)$ is 5. The first minimum in the plot between AMI and τ occurs at 35th sample, which implies the optimal time delay τ should be 35. It should be noted that as long as τ is reasonably close to the optimal value and d_E is sufficiently large, the reconstructed state space will exhibit same dynamical properties as the original dynamical system. Thus, the results of local and orbital stability analyses will be robust to moderate changes in those parameters.

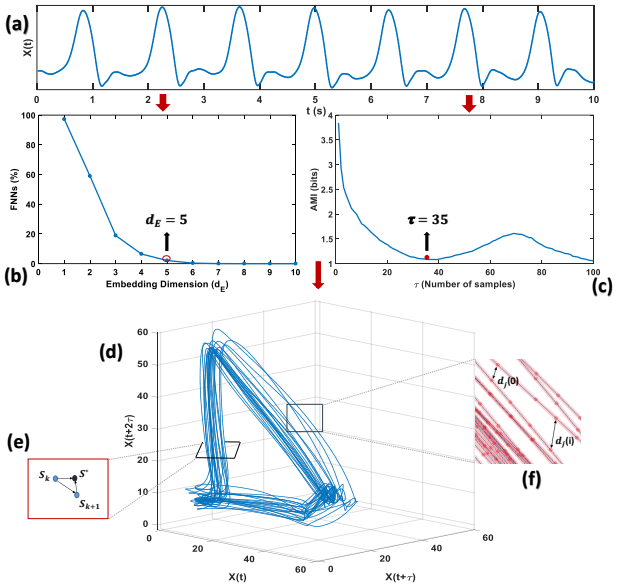

Fig. 3. The representation of FM and λ calculation from the kinematic time series data: (a) sample knee joint time series data, (b-c), the FNNs and AMI plots resulting from the time series, to calculate the proper embedding dimension (d_E) and time delay (τ), (d) the three dimensional view of the reconstructed state space from the time delayed copies of the time series data (the original state space is 5 dimensional), (e) representation of a Poincaré section, transecting the state space perpendicular to the system trajectory. The Floquet multipliers quantify how the distance between system states at consecutive strides, S_k and S_{k+1}, evolves with regard to the fixed point, S^*, (f) divergence of the distance between neighbouring trajectories which will be reflected by λ values.

2) Local stability: The local stability measure provides a direct way to analyze the chaotic order of the system using finite-time divergence exponents. The local stability is quantified by estimating the average exponential rates of divergence of initially neighboring trajectories in state space as they evolve over time. These local divergence exponents provide a measure of the system's sensitivity to local perturbations. Positive exponents indicate local instability and larger exponents indicate greater sensitivity to local perturbations.

The nearest neighbor points in adjacent trajectories in the reconstructed state space represent the effects of small local perturbations of the system. The average exponential divergence for each embedded time series is provided by the algorithm given in [31]. The Euclidean distance between neighboring trajectories is computed as a function of time and averaged overall original pairs of initially nearest neighbors. The local divergence exponents (λ) are estimated from the slopes of linear fits to these exponential divergence curves.

$$y(i) = \frac{1}{\Delta t} < \ln[d_j(i)] >, \quad (3)$$

where $d_j(i)$ is the Euclidean distance between jth pair of the initially nearest neighbors after i time steps (i.e. $i\Delta t$ seconds) as shown in Fig. 3(f), and $< \cdot >$ denotes average over all

pairs of j. The short-term exponent (λ_s) is calculated from the slopes of linear fits to the divergence curve between 0 to 1 stride and the long-term exponent (λ_l) is calculated between 4 and 10 strides [32].

3) Orbital stability: The orbital stability concept is based on the assumption that the human gait has a fixed period. It is defined using FMs that quantify, discretely from one gait cycle to the next, the tendency of the system's state to return to the periodic limit cycle orbit after small perturbation [33]. FMs are the eigenvalues of the Jacobian of the Poincaré map. The first step for calculating the FMs is to normalize the state-space data of each stride to 101 samples (0-100% gait cycle) [34]. This will allow us to define 101 Poincaré maps for the system as

$$S^l_{k+1} = F(S^l_k) \tag{4}$$

where k is the index of the individual strides, l is the index over the Poincaré sections (% gait cycle), and S^l_k represents the d_E dimensional system states for the lth point in the normalized time within the kth gait cycle. Limit cycle trajectories that correspond to single fixed points in each Poincaré map is

$$S^l_* = F(S^l_*) \tag{5}$$

For walking data, fixed points at each Poincaré section (i.e. each % of the gait cycle) are defined by the average trajectory across all the strides within a trail. Orbital stability at each Poincaré section estimates the effect of a small perturbation away from these fixed points, using a linear approximation of (5) given by

$$[S^l_{k+1} - S^l_*] = J(S^l_*)[S^l_k - S^l_*] \tag{6}$$

where $J(S^l_*) \in \mathbb{R}^{d_E \times d_E}$ is the Jacobian matrix of the system at each Poincaré section. The FMs are the eigenvalues of $J(S^l_*)$. Therefore, the condition for the limit cycle to be orbitally stable is that the complex valued FMs must have magnitude < 1. A limit cycle with any FM with magnitude > 1 is considered orbitally unstable. For statistical analysis, first the FMs with maximum magnitude are computed at each Poincaré section (% of the gait) as FM^l. Next, we find the maximum of FMs across the Poincaré sections:

$$\text{max FM} = \max_{l=0,1,\ldots,100} FM^l \tag{7}$$

which represents the most unstable instant within a gait cycle.

4) Variability: The measured variability in the complex dynamical system may arise from the deterministic dynamics of the system itself (such as a chaotic attractor, which is the case for human gait). In such cases, variability is just a reflection of multiple degrees of freedom available to the system and does not imply destabilization of the system. Although the variability in the biological system is likely to obtain from either noise or deterministic sources, it is difficult to separate them. However, on a pragmatic level, the variability is critical to the stability of the walking because it gives insights regarding state deviation which may lead to falling. In general, MAD is more robust than the standard deviation (SD), and is thus a good choice to use as an indicator of variability [35]. For continuous variables such as joint angle time series, they are first separated into individual strides. These individual strides are then normalized (0-100%) over time and aligned. For each of the aligned time intervals, the variability is then calculated using the MAD metric [35],

$$MAD(X) = med(|X - med(X)\vec{\mathbf{1}}|), \tag{8}$$

where $X \in \mathbb{R}^{101}$ is the sample (i.e., aligned joint angles for each stride, 101 points), $med(X) \in \mathbb{R}$ is the median of the sample, and $\vec{\mathbf{1}} \in \mathbb{R}^{101}$ is the all-ones vector.

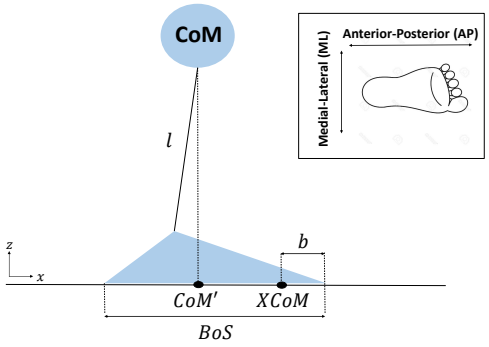

Fig. 4. Schematic representation of the inverted pendulum model to calculate the minimum margin of stability (b_{min}) in AP direction.

B. Measures from Biomechanical Principles

The extrapolated center of mass ($XCoM$) method extends the condition of the static equilibrium of the inverted pendulum model, in which the CoM must be positioned over the base of support (BoS) by adding a linear function of the velocity of the CoM to the CoM position [36]. BoS is defined as the area to which the center of pressure (CoP) is confined. In theory, this method describes how close an inverted pendulum is to falling, given the position and velocity of its CoM, and the position of the boarder of its BoS (BoS), as shown in Fig. 4. The $XCoM$ can be used to calculate the spatial margin of stability "b". The margin of stability refers to the distance between $XCoM$ and BoS. The calculation is derived in [36] for unperturbed walking. Given the position and velocity of the CoM, the $XCoM$ can be calculated as:

$$XCoM = CoM' + \frac{V_{CoM'}}{\omega_0} \tag{9}$$

$$\omega_0 = \sqrt{\frac{g}{l}} \tag{10}$$

where CoM' is the vertical projection of the CoM on the ground (shown in Fig. 4). $V_{CoM'}$ is the velocity of CoM', ω_0 is the pendulum eigenfrequency, g is the acceleration of gravity, and l is the pendulum effective length. The margin of stability can be defined as:

$$b = BoS - XCoM \tag{11}$$

here BoS refers to the boarder of BoS. b is a representative of the maximum perturbation to the CoM before the inverted pendulum becomes unstable (CoM moving past the BoS). The minimum of b (b_{min}) shows the most unstable point within a step [36].

For the calculation of margin of stability, the positions of CoM' and BoS need to be determined. The CoP is estimated using the force measurements from the instrumented treadmill. During walking, only the lateral and anterior boundaries of the BoS need to be known [19]. Here we defined BoS as the extreme lateral and anterior values of CoP for each leg within each gait cycle. The CoM' can be estimated by filtering the CoP as given in [37].

IV. Results

A. Orbital and Local Stability

1) Orbital stability results: Six time series of joint angles, i.e., bilateral hip, knee, and ankle were considered. Using GFNN, the embedding dimension (d_E) for the state space reconstruction was found to be five for all the cases. The embedded state space for each time series exhibited a strong periodic structure with an expected stride to stride variability during walking. For computing the FM values, time series of joint angles from 100 continuous strides were used. These strides were taken from the middle of the session by removing the first and last 30 seconds of data.

Three-way analysis of variance (ANOVA) model is performed with three factors: participants, conditions, and joint segments. Statistical significance is evaluated at $p < 0.05$. The interaction model computes the p values on three main effects (participants, conditions, segments) and three two-factor interaction effects. Here, the null hypothesis for the main effect states that all group max FMs are equal for each individual factor. The alternate hypothesis states that at least one group max FM is different. For example, consider segments as the factor and six joint segments as distinct groups. The null hypothesis were to be rejected if the max FM of at least one segment is different from those of other segments. For two-factor interaction effects, the null hypothesis were to be rejected if at least one interaction term was not equal to zero.

For max FMs, it is found that all the three main effects and three two-factor interaction effects are statistically significant. This result states that participants, conditions, and segments affect the max FM. However, this three-way ANOVA does not specify how the max FM varies across different conditions. As the focus of this work is to evaluate the impact of proposed strategy (AIT) on stability, normal against AIT and FSM against AIT were picked for one-way ANOVA. For each joint segment, one-way ANOVA was performed on eleven participants' max FMs using normal and AIT conditions as grouping variables, and same analysis was performed to compare between FSM and AIT.

The mean and SD of max FMs of six segments for eleven healthy participants in five conditions are displayed in Fig. 5(a). For one-way ANOVA, $p < 0.05$ suggested statistical significance. In Fig. 5(a), a "$*$" is marked on left hip, left knee, right hip, and right knee, showing the statistically significant result in one-way ANOVA between normal and AIT conditions for those joints. It demonstrates that the mean of max FMs (across eleven participants) for normal and AIT conditions are different. For the ANOVA across FSM and AIT, the statistically significant result is observed only for the left hip and right hip. Whereas, for the other segments, the max FMs means are not significantly different between FSM and AIT.

From three-way ANOVA, it is found that the interaction between participants and conditions is statistically significant for max FMs. Therefore, participant$\times$condition interaction plots are given for all the six joints in Figs. 5(b) and 5(c). Fig. 5(b) demonstrates that max FMs in AIT and FSM conditions are lower than normal walking for all the left leg joints. Whereas, passive and ZI cases exhibit higher max FM values than normal walking. This similar trend is observed on the right-side joint segments for passive and ZI cases in Fig. 5(c). However, the max FMs for AIT and FSM are slightly higher than normal walking for the right leg joints. We expect that wearing KAD may increase the max FM compared to the normal walking due to the weight of KAD. The passive and ZI conditions exhibit higher max FMs for both legs. In general, AIT lead to lower max FM when compared to FSM for all joint segments which can be observed in Figs. 5(b) and 5(c). However, the ANOVA yielded statistical significant result only for left and right hips.

2) Local stability results: The algorithm to compute divergence exponents λ_s and λ_l was shown to be robust for small data sets [31]. The extracted 100 continuous strides were first divided into 33, 33, and 34 strides. Then, λ_s (0 and 1 stride) and λ_l (4 and 10 strides) were computed for all six joints for these 3 stride blocks and then averaged to obtain the final λ_s and λ_l. The three-way and one-way ANOVA were performed on λ_s and λ_l in the similar fashion as on max FM in section IV-A.1. For three-way ANOVA about λ_s, the statistical significance was observed for all the three main factors and three two-way interactions. Whereas, for λ_l, the statistical significance was observed for the three main factors and only one two-factor interaction effect (participant$\times$segment).

Figure 6 shows that the local divergence exponents λ_s and λ_l exhibit positive divergence values for all the five cases, which indicates that the system is chaotic in nature. A higher divergence value means a higher order of the chaotic system. For one-way ANOVA, it can be seen in Fig. 6(a) that the λ_s estimates are statistically significant for left hip, left knee, right hip, and right knee when comparing between normal and AIT conditions. Similar to max FMs, the participant$\times$condition interaction is statistically significant for λ_s. Also, they follow a similar trend to that of the max FMs that λ_s values in FSM and AIT conditions are lower than normal walking, and λ_s values in passive and ZI are higher than normal walking for left leg. Whereas, λ_s values are slightly higher in FSM and AIT compared to normal walking for the right leg, as displayed in Figs. 6(b) and 6(c).

The statistical significance for λ_l can be seen in left hip, left knee, left ankle, right hip, and right ankle when comparing AIT and normal walking conditions, as shown in Fig. 6(d). The participant$\times$condition interaction is found to be not statistically significant using three-way ANOVA. Nevertheless, this two-way interaction plot for eleven participants is displayed in Figs. 6(e) and 6(f). Although it can be visualized from Figs. 6(e) and 6(f) that λ_l values are different for participants for different conditions, however, it is found from ANOVA analysis that the interaction is not statistically significant.

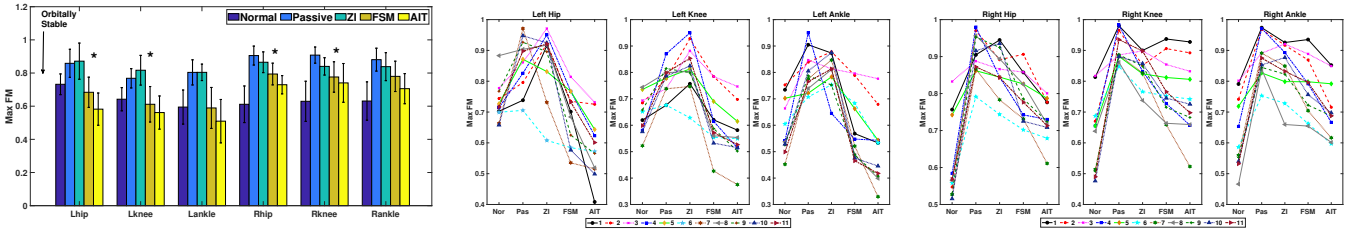

(a) max FM for five conditions. (b) max FMs for eleven participants (left side). (c) max FMs for eleven participants (right side).

Fig. 5. Orbital stability results of six segments for eleven participants during five conditions. (a) The mean and SD of max FMs of six joint segments were displayed. A statistically significant difference in max FMs between normal and AIT conditions is indicated with '*' for the specific joint. The variation in max FMs of left and right leg joint segments for each participant during five conditions is displayed in (b) and (c), respectively.

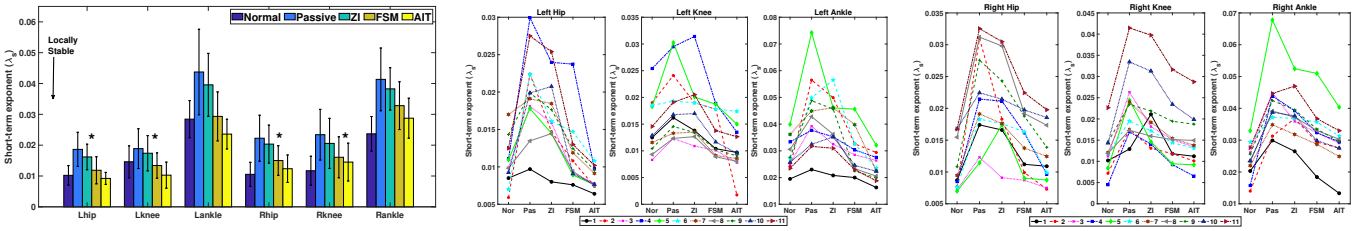

(a) Short-term exponent (λ_s) for five conditions. (b) λ_s for eleven participants (left side). (c) λ_s for eleven participants (right side).

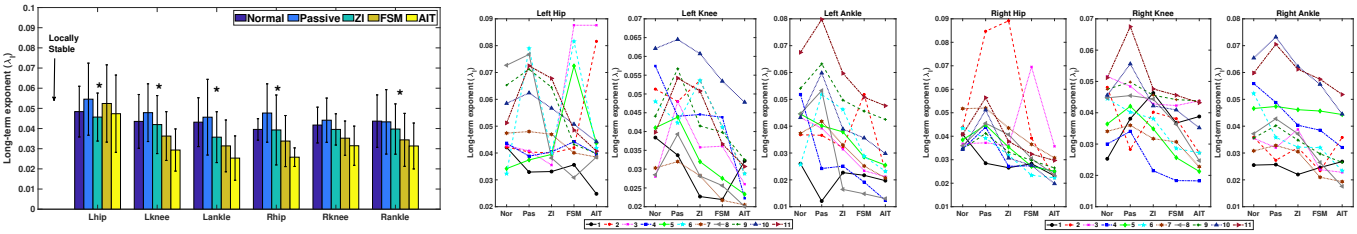

(d) Long-term exponent (λ_l) for five conditions. (e) λ_l for eleven participants (left side). (f) λ_l for eleven participants (right side).

Fig. 6. Local stability results of six segments for eleven participants during five conditions. (a) and (d): the mean and SD of $\boldsymbol{\lambda_s}$ and $\boldsymbol{\lambda_l}$ of six joint segments were displayed. Statistically significant difference in $\boldsymbol{\lambda_s}$ and $\boldsymbol{\lambda_l}$ between normal and AIT conditions is indicated with '*' for the special joint. The variation in $\boldsymbol{\lambda_s}$ and $\boldsymbol{\lambda_l}$ of left and right leg joint segments for each participant during five conditions is displayed in (b) and (e), (c) and (f), respectively.

Comparing between Figs. 5(a), 6(a) and 6(d), the trend of λ_l is quite different from that of max FM and λ_s, as λ_l values are lower for ZI, FSM, and AIT conditions compared to normal walking for five joint segments except left hip. Whereas, max FM and λ_s values are lower for AIT and FSM when compared to normal walking for left leg segments and slightly higher for right leg segments.

For one-way ANOVA comparing FSM and AIT, the λ_s values are statistically significant in left hip and left ankle. Whereas, for λ_l values, there is no statistical significance for any of the joint segments. All participants exhibited positive local divergence exponents which implies that they are locally unstable. A larger positive value means more locally unstable. From Fig. 6, it is clear that the participants were least locally unstable in the AIT and normal walking conditions for the left and right legs, respectively. Moreover, from λ_s results it is inferred that for most of the participants, both sides are less locally unstable in the AIT condition compared to FSM, as shown in Figs. 6(b) and 6(c). λ_l results show that the participants are locally less unstable for all the joint segments except left hip in AIT compared to the other four conditions. The stability studies reported in [11] suggest that λ_s correlates well with the probability of falling in comparison with λ_l. Therefore, the inferences of the local stability in this study are made from λ_s estimates.

B. Variability Results

The stride to stride variability was evaluated for six joint segments across all the conditions in 11 participants.The mean and SD of six joint angles are displayed in Table II, and AIT exhibits less MAD values for all the joints compared to the other four conditions. For each segment, one-way ANOVA analysis was performed on MAD values comparing normal and AIT conditions. It is shown in Table II that MAD values are significantly different for all joint segments except the right knee when comparing normal and AIT conditions. It is noticed that the MAD mean is considerably higher than that of the left knee in AIT the condition. A possible explanation is that the participants tried to adjust to the assistance provided to the right knee, causing larger variance in the right knee motion and making the MAD value similar to the normal walking case. More studies are needed to understand the inter-joint coordination and explain the MAD patterns. For the ANOVA comparing between FSM and AIT, the MAD values

TABLE II
THE MEAN AND SD OF MAD (VARIABILITY) FOR 11 PARTICIPANTS (SEGMENT×CONDITION). "*" INDICATES STATISTICALLY SIGNIFICANT DIFFERENCE BETWEEN NORMAL AND AIT CONDITIONS ($p < 0.05$).

segment	Normal	Passive	ZI	FSM	AIT
Left hip°*	**0.89±0.138**	0.94±0.197	1.26±0.721	0.83±0.158	**0.71±0.130**
Left knee°*	**1.55±0.209**	1.44±0.329	1.72±0.665	1.29±0.310	**1.14±0.183**
Left ankle°*	**0.96±0.183**	0.93±0.349	1.18±0.556	0.78±0.131	**0.68±0.097**
Right hip°*	**1.37±0.346**	1.46±0.434	1.16±0.205	1.39±0.456	**0.95±0.236**
Right knee°	**1.74±0.386**	2.12±0.279	2.15±0.479	2.31±0.538	**1.58±0.204**
Right ankle°*	**1.57±0.373**	1.39±0.380	1.21±0.322	1.31±0.452	**0.95±0.182**

are statistically significant in the three joint segments on the right side only. The MAD values are higher for the right knee compared to the other five joints because the weight of the KAD influences the right knee joint's range of motion (ROM) and increases variability. This increased variability also implies changes in the knee joint torques and loads over a gait cycle. Comparing MAD values between normal walking and AIT, it is clear that the KAD reduces kinematic variability of the participants in AIT.

It will be useful to quantify gait symmetry to understand the variability. In this paper, stance time is used to derive gait symmetry index (GSI), since the KAD provides assistance during stance phase. The Robinson index is used [38]

$$\text{GSI} = \frac{x_r - x_l}{\max(x_r, x_l)} \times 100 \tag{12}$$

x_r and x_l are the average right leg stance time and average left leg stance time for 11 participants, each with 100 strides, given in seconds. The ideal GSI for perfectly symmetrical gait should be equal to 0. However, it is difficult even for healthy participants to achieve perfectly symmetrical gait. In a study performed on 58 healthy participants during overground walking, a mean GSI value of 2.38 was reported using stance time [39]. In this study, the GSI computed for normal, passive, ZI, FSM and AIT are 1.96, 3.82, 3.63, 2.94, and 2.26, respectively. The GSI value for normal walking is low when compared to the mean GSI value reported in [39]. This may be due to the controlled walking environment, i.e., treadmill, which was shown to reduce GSI values compared to overground walking [40]. It is clear from the GSI values that the participants' gait is more symmetric in the AIT condition compared to passive, ZI and FSM conditions.

C. Extrapolated XCoM (Margin of Stability) Results

The extrapolated center of mass ($XCoM$) concept was used to study the stability in both mediolateral (ML) and anteroposterior (AP) directions. In general, b_{min} values are negative in the AP direction, implying that stability cannot be recovered without moving the arms, trunk, or the use of a stepping strategy [11], which are not considered in the inverted pendulum model [36]. The mean and SD of b_{min} values for all participants in both ML and AP directions are plotted in Fig. 7. The AP stability results are statistically significant with respect to both participants and conditions, respectively. Whereas, the ML stability results are statistically significant with respect to only the participant, meaning the

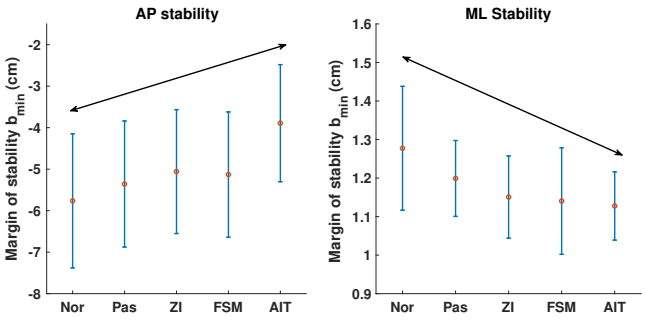

Fig. 7. The mean and SD of margin of stability (b_{min}) values in both ML and AP directions for 11 participants for five conditions.

condition was not a significant factor in ML direction. It can be seen from Fig. 7 that b_{min} mean value is lower in the AIT condition compared to other cases in AP direction which means participants in AIT exhibit less instability compared to other cases. The margin of stability result shows that normal walking is the most unstable case in the AP direction, and wearing KAD, especially in an active mode, will reduce the AP instability. However, in the ML direction, the difference of b_{min} values in different conditions is not significant. This is expected as the assistive torque is in AP direction, and the only perturbation in ML direction comes from the weight of KAD. The trends of stability in AP and ML directions are represented by double-sided arrows in Fig. 7.

V. DISCUSSION

A. Assessment and Comparison of Stability Metrics

In literature, max FMs and λ_s correlated well with the probability of falling in various studies [11]. Therefore, max FMs and λ_s metrics are evaluated to assess the dynamic gait stability of the human-KAD system. Whereas, the λ_l has been used as a measure to study chaotic orders and variability in the system in most studies [11]. MAD is a direct measure of gait variability.

In this study, participants maintain similar local and orbital stability behavior for all six joint segments, as shown by the trend of mean max FM and mean λ_s for five conditions in Figs. 5(a) and 6(a). The difference of max FM and λ_s between AIT and normal condition are significant for all the joint segments except right and left ankle. Both max FM and λ_s suggest that left hip and left knee are more stable than right hip and right knee during active KAD cases (AIT and FSM) when compared to the normal walking as shown in Figs. 5(a) and 6(a). Except for the left hip, both the mean λ_l and MAD are lower for AIT when compared to normal walking. Also, the mean λ_l is lower for the active cases compared to normal walking. However, for λ_s and max FM of the right leg, normal walking has the lowest values compared to all other cases.

In order to see if there exist any correlation between pairs of stability metrics, coefficients of determination (r^2) are calculated for the following pairs: FM×λ_s, FM×MAD, λ_s×MAD, MAD×λ_l. The correlation tests were conducted separately once for each condition and once for each segment. To evaluate the reliability of the linear model with a limited

number of sample data, the statistical significance of the correlation coefficient is also reported. The statistical significance is judged based on Bonferroni correction $p < 0.05/30$ where 30 is the number of segments (6) $\times$ the number of conditions (5). This hypothesis test will determine if there exists a correlation coefficient different from zero, out of the sample data.

The correlations were not strong as $r^2 < 20\%$ for all pairs of stability metrics. Also no significant correlation were observed ($p > 0.05/30$). This result highlight the fact that the metrics are independent and each represents a certain feature of the system. λ_s describes local stability within a step while max FM describes orbital stability between steps. Whereas, the λ_l and MAD are used to study how the chaotic order and variability of the joint segments change with respect to the perturbations. This study shows that there is no direct relationship between variability and stability of the human gait. More variability in the human gait does not mean that the gait is unstable or vice versa. All the reported metrics have their individual significance and there exists no strong correlation between the metrics. The results given in Section IV display useful insights related to the variation of stability metrics during various conditions with KAD.

B. The Effects of Unilateral Assistance

The unilateral assistance to a specific joint will help us understand intra and inter joint behaviors. It can be seen from Figs. 5(a) and 6(a) that max FM and λ_s for assisted conditions (FSM and AIT) are lower than normal walking for the left (unassisted) leg. Whereas, for the right leg, AIT and FSM exhibit slightly higher max FM and λ_s than normal walking. The max FM and λ_s show a similar trend for all five conditions. This result can be analyzed from the human locomotor adaption paradigm, and many studies were conducted to examine bilateral responses subjected to unilateral limb perturbations [41], [42]. It was shown that such perturbation produced bilateral kinematic changes and evoked contralateral leg responses. In [42], the unilateral stiffness perturbations using variable stiffness treadmill evoked repeatably and scalably muscle activities and kinematic response of the contralateral leg. Also, they provided strong evidence that supra-spinal activity could be evoked by inducing unilateral stiffness perturbations. These studies provide experimental evidence that human neuromusculoskeletal system adapts to unilateral perturbations in such a way that it compensates for the perturbations by responses from the unperturbed leg. In our case, it is possible that participants adopted a similar strategy to compensate for the perturbations on the right leg by altering left leg's patterns. As an adaptation strategy, the responses from the unassisted leg would acquire both feedback and feedforward mechanisms to counteract perturbations to the right leg. In passive and ZI cases, the KAD adds an extra weight of 2.3 kg to the right leg but not providing assistance, which could cause discomfort to the participants. This is similar to the studies performed in the past by adding weight to a limb to provide resistance while walking [43]. The bilateral adaptation is observed, which shows variability in kinematics. Therefore, max FM and λ_s are generally higher for both legs in passive and ZI conditions. Smooth transition of robot impedance values between gait phases in the AIT mode leads to lower values in λ_s and max FM for both legs, compared to FSM.

C. Limitations of this Study

Based on the results obtained in our prior work [25], in this study, each participant's unique impedance parameters were used for the KAD controller to evaluate the gait stability. However, the robustness of the gait stability results with variations of robot impedance parameters was not evaluated. Moreover, the muscle activities of lower-limb muscles were not recorded in this study. Those muscular responses may give more insights and explanations of the dynamic gait stability results. They may also help us understand how the participants apply the compensatory actions in response to perturbations with the unassisted leg at the muscular level. Lastly, the overground experiments were not conducted in this study due to space limits. It is expected that participants exhibit higher variability during overground walking.

VI. Conclusion

In this paper, the dynamic gait stability of the human-LEAD system subjected to unilateral knee assistance was studied in five test conditions. The participants in the AIT condition exhibited higher dynamic stability on the left side in terms of max FM and λ_s compared to the other four conditions. Whereas, for the right (assisted) side, higher dynamic stability is observed in normal walking. Moreover, participants showed higher gait dynamic stability on both sides in AIT compared to FSM, which could be attributed to the smooth impedance transition between gait phases. The metrics λ_l and MAD showed that participants exhibited less kinematic variability in AIT compared to normal walking, for both sides.

For future work, a bipedal simulation framework will be developed in which the bipedal model parameters will be designed based on participant's anthropometric data. We will assess the dynamic gait stability and variability of bipedal walking, and compare them with experimental results. Future work will also study the muscular-level responses to unilateral assistance. This will help us understand how humans adapt to assistance and optimize their gait patterns. Patients will be recruited to study their walking patterns with and without assistance, to evaluate the gait stability performance of different robot controllers. Similar analysis with a soft robotic exosuit [44] will also be conducted to extend the results of this study to other types of assistive devices.

References

[1] N. D. o. E. United Nations, New York and S. Affairs, *World population ageing, 1950-2050*. United Nations Publications, 2002.

[2] M. Tieland, I. Trouwborst, and B. C. Clark, "Skeletal muscle performance and ageing," *Journal of cachexia, sarcopenia and muscle*, vol. 9, no. 1, pp. 3–19, 2018.

[3] W. Deng, I. Papavasileiou, Z. Qiao, W. Zhang, K.-Y. Lam, and H. Song, "Advances in automation technologies for lower-extremity neurorehabilitation: A review and future challenges," *IEEE Reviews in Biomedical Engineering*, 2018.

[4] A. J. Young and D. P. Ferris, "State of the art and future directions for lower limb robotic exoskeletons," *IEEE Transactions on Neural Systems and Rehabilitation Engineering*, vol. 25, no. 2, pp. 171–182, 2017.

[5] T. Yan, M. Cempini, C. M. Oddo, and N. Vitiello, "Review of assistive strategies in powered lower-limb orthoses and exoskeletons," *Robotics and Autonomous Systems*, vol. 64, pp. 120–136, 2015.

[6] G. F. Fuller, "Falls in the elderly." *American family physician*, vol. 61, no. 7, pp. 2159–68, 2000.

[7] S. M. R. Sorkhabadi, "Gait dynamic stability analysis with wearable assistive robots," Master's thesis, Arizona State University, 2018.

[8] J. M. Hausdorff, C. Peng, Z. Ladin, J. Y. Wei, and A. L. Goldberger, "Is walking a random walk? evidence for long-range correlations in stride interval of human gait," *Journal of Applied Physiology*, vol. 78, no. 1, pp. 349–358, 1995.

[9] U. H. Buzzi, N. Stergiou, M. J. Kurz, P. A. Hageman, and J. Heidel, "Nonlinear dynamics indicates aging affects variability during gait," *Clinical biomechanics*, vol. 18, no. 5, pp. 435–443, 2003.

[10] R. T. Harbourne and N. Stergiou, "Movement variability and the use of nonlinear tools: principles to guide physical therapist practice," *Physical therapy*, vol. 89, no. 3, pp. 267–282, 2009.

[11] S. Bruijn, O. Meijer, P. Beek, and J. Van Dieën, "Assessing the stability of human locomotion: a review of current measures," *Journal of the Royal Society Interface*, vol. 10, no. 83, p. 20120999, 2013.

[12] J. Dingwell, J. Cusumano, D. Sternad, and P. Cavanagh, "Slower speeds in patients with diabetic neuropathy lead to improved local dynamic stability of continuous overground walking," *Journal of biomechanics*, vol. 33, no. 10, pp. 1269–1277, 2000.

[13] T. E. Lockhart and J. Liu, "Differentiating fall-prone and healthy adults using local dynamic stability," *Ergonomics*, vol. 51, no. 12, pp. 1860–1872, 2008.

[14] P. M. McAndrew, J. M. Wilken, and J. B. Dingwell, "Dynamic stability of human walking in visually and mechanically destabilizing environments," *Journal of biomechanics*, vol. 44, no. 4, pp. 644–649, 2011.

[15] A. H. Nayfeh and B. Balachandran, *Applied nonlinear dynamics: analytical, computational, and experimental methods*. John Wiley & Sons, 2008.

[16] K. P. Granata and T. E. Lockhart, "Dynamic stability differences in fall-prone and healthy adults," *Journal of Electromyography and Kinesiology*, vol. 18, no. 2, pp. 172–178, 2008.

[17] K. S. van Schooten, L. H. Sloot, S. M. Bruijn, H. Kingma, O. G. Meijer, M. Pijnappels, and J. H. van Dieën, "Sensitivity of trunk variability and stability measures to balance impairments induced by galvanic vestibular stimulation during gait," *Gait & posture*, vol. 33, no. 4, pp. 656–660, 2011.

[18] J. B. Dingwell, J. John, and J. P. Cusumano, "Do humans optimally exploit redundancy to control step variability in walking?" *PLoS computational biology*, vol. 6, no. 7, p. e1000856, 2010.

[19] P. M. M. Young, J. M. Wilken, and J. B. Dingwell, "Dynamic margins of stability during human walking in destabilizing environments," *Journal of biomechanics*, vol. 45, no. 6, pp. 1053–1059, 2012.

[20] C. Duclos, P. Desjardins, S. Nadeau, A. Delisle, D. Gravel, B. Brouwer, and H. Corriveau, "Destabilizing and stabilizing forces to assess equilibrium during everyday activities," *Journal of biomechanics*, vol. 42, no. 3, pp. 379–382, 2009.

[21] P. Antonellis, S. Galle, D. De Clercq, and P. Malcolm, "Altering gait variability with an ankle exoskeleton," *PloS one*, vol. 13, no. 10, p. e0205088, 2018.

[22] J. A. Norris, A. P. Marsh, K. P. Granata, and S. D. Ross, "Positive feedback in powered exoskeletons: Improved metabolic efficiency at the cost of reduced stability?" in *ASME 2007 International Design Engineering Technical Conferences and Computers and Information in Engineering Conference*, 2007, pp. 1619–1626.

[23] G. Zeilig, H. Weingarden, M. Zwecker, I. Dudkiewicz, A. Bloch, and A. Esquenazi, "Safety and tolerance of the rewalk™ exoskeleton suit for ambulation by people with complete spinal cord injury: a pilot study," *The journal of spinal cord medicine*, vol. 35, no. 2, pp. 96–101, 2012.

[24] S. A. Kolakowsky-Hayner, J. Crew, S. Moran, and A. Shah, "Safety and feasibility of using the eksotm bionic exoskeleton to aid ambulation after spinal cord injury," *J Spine*, vol. 4, p. 003, 2013.

[25] P. T. Chinimilli, Z. Qiao, S. M. R. Sorkhabadi, V. Jhawar, I. H. Fong, and W. Zhang, "Automatic virtual impedance adaptation of a knee exoskeleton for personalized walking assistance," *Robotics and Autonomous Systems*, vol. 114, pp. 66–76, April 2019.

[26] P. T. Chinimilli, S. W. Wachtel, P. Polygerinos, and W. Zhang, "Hysteresis compensation for ground contact force measurement with shoe-embedded air pressure sensors," in *ASME 2016 Dynamic Systems and Control Conference*, 2016, pp. V001T09A006–V001T09A006.

[27] P. T. Chinimilli, S. Redkar, and W. Zhang, "Human activity recognition using inertial measurement units and smart shoes," in *American Control Conference (ACC), 2017*, 2017, pp. 1462–1467.

[28] A. Pagel, R. Ranzani, R. Riener, and H. Vallery, "Bio-inspired adaptive control for active knee exoprosthetics," *IEEE Transactions on Neural Systems and Rehabilitation Engineering*, vol. 25, no. 12, pp. 2355–2364, 2017.

[29] E. H. Sinitksi, K. Terry, J. M. Wilken, and J. B. Dingwell, "Effects of perturbation magnitude on dynamic stability when walking in destabilizing environments," *Journal of biomechanics*, vol. 45, no. 12, pp. 2084–2091, 2012.

[30] H. Kantz and T. Schreiber, *Nonlinear time series analysis*. Cambridge university press, 2004, vol. 7.

[31] M. T. Rosenstein, J. J. Collins, and C. J. De Luca, "A practical method for calculating largest lyapunov exponents from small data sets," *Physica D: Nonlinear Phenomena*, vol. 65, no. 1-2, pp. 117–134, 1993.

[32] J. Dingwell, J. Cusumano, P. Cavanagh, and D. Sternad, "Local dynamic stability versus kinematic variability of continuous overground and treadmill walking," *Journal of biomechanical engineering*, vol. 123, no. 1, pp. 27–32, 2001.

[33] Y. Hurmuzlu and C. Basdogan, "On the measurement of dynamic stability of human locomotion," *Journal of biomechanical engineering*, vol. 116, no. 1, pp. 30–36, 1994.

[34] J. B. Dingwell and H. G. Kang, "Differences between local and orbital dynamic stability during human walking," *Journal of biomechanical engineering*, vol. 129, no. 4, pp. 586–593, 2007.

[35] T. Chau, S. Young, and S. Redekop, "Managing variability in the summary and comparison of gait data," *Journal of neuroengineering and rehabilitation*, vol. 2, no. 1, p. 22, 2005.

[36] A. Hof, M. Gazendam, and W. Sinke, "The condition for dynamic stability," *Journal of biomechanics*, vol. 38, no. 1, pp. 1–8, 2005.

[37] A. L. Hof, R. M. van Bockel, T. Schoppen, and K. Postema, "Control of lateral balance in walking: experimental findings in normal subjects and above-knee amputees," *Gait & posture*, vol. 25, no. 2, pp. 250–258, 2007.

[38] S. Viteckova, P. Kutilek, Z. Svoboda, R. Krupicka, J. Kauler, and Z. Szabo, "Gait symmetry measures: A review of current and prospective methods," *Biomedical Signal Processing and Control*, vol. 42, pp. 89–100, 2018.

[39] M. Błażkiewicz, I. Wiszomirska, and A. Wit, "Comparison of four methods of calculating the symmetry of spatial-temporal parameters of gait," *Acta of bioengineering and biomechanics*, vol. 16, no. 1, 2014.

[40] D. Gouwanda, "Comparison of gait symmetry indicators in overground walking and treadmill walking using wireless gyroscopes," *Journal of Mechanics in Medicine and Biology*, vol. 14, no. 01, p. 1450006, 2014.

[41] J. T. Choi and A. J. Bastian, "Adaptation reveals independent control networks for human walking," *Nature neuroscience*, vol. 10, no. 8, p. 1055, 2007.

[42] J. Skidmore and P. Artemiadis, "Unilateral floor stiffness perturbations systematically evoke contralateral leg muscle responses: a new approach to robot-assisted gait therapy," *IEEE Transactions on Neural Systems and Rehabilitation Engineering*, vol. 24, no. 4, pp. 467–474, 2016.

[43] A. Blanchette and L. J. Bouyer, "Timing-specific transfer of adapted muscle activity after walking in an elastic force field," *Journal of neurophysiology*, vol. 102, no. 1, pp. 568–577, 2009.

[44] S. Sridar, Z. Qiao, N. Muthukrishnan, W. Zhang, and P. P. Polygerinos, "A soft-inflatable exosuit for knee rehabilitation: Assisting swing phase during walking," *Frontiers in Robotics and AI*, vol. 5, p. 44, 2018.